Jurnal Mekanikal
December 2006, No. 22, 115-131

EFFECT OF LOADING FREQUENCY ON FATIGUE BEHAVIOR OF MAGNESIUM ALLOY IN HUMID ENVIRONMENT

Zainuddin Sajuri*
Department of Mechanical and Materials Engineering
Faculty of Engineering
Universiti Kebangsaan Malaysia
43600 Bangi, Selangor, Malaysia

Yukio Miyashita and Yoshiharu Mutoh
Department of Mechanical Engineering
Nagaoka University of Technology
Kamitomioka-machi 1603-1, Nagaoka, 940-21 Japan

ABSTRACT

Effect of loading frequency on fatigue behavior of an extruded AZ61 magnesium alloy was investigated at 50℃-80%RH environment. The frequencies applied were 1 and 10 Hz. It was found that at stresses below the fatigue limit (at 20℃-55%RH), the fatigue fracture was time dependent where fatigue lives for both frequencies were almost identical. In contrast, the fatigue fracture in the region higher than the fatigue limit was dominated by the number of loading cycles. Fatigue fracture at low stress amplitudes for both frequencies were originated from the corrosion pit formed on the surface. Effect of frequency on fatigue crack growth behavior was also investigated. The results showed that in the near-threshold region, the 1 Hz frequency demonstrated higher fatigue crack growth resistance compared to the 10 Hz.

Keywords: *Fatigue, frequency, environment, corrosion pit, magnesium alloy.*

1.0 INTRODUCTION

Applications in aerospace and automobile industries have always encouraged the search and development of new lightweight materials in order to enhance the efficiency and the performance of the components. Nowadays, the cost reduction for space and ground vehicles has become one of the major considerations in many air and land transportation companies. Nearly every

* Corresponding author: E-mail: sajuri@vlsi.eng.ukm.my

effort for weight reduction is economically worthwhile, especially for the substitution of metals by lightweight alloys [1]. Among the lightweight alloys, magnesium, aluminum and titanium alloys are known for the benefits derived from the reduction in weight of components and their high performance especially in aircrafts.

For many years, magnesium alloys, the lightest structural materials, have been attractive to engineers due to their low density (1.74 g/cm^3) compared to other counterparts such as aluminum and titanium alloys. In fact, magnesium alloys have been widely used in aircraft and automobile industries in 1940's to 1950's [2,3]. However, the requirement for high strength in addition to high corrosion resistance for applications in aerospace and automobile industries has limited the use of conventional magnesium alloys. In recent years, the potential for applications of magnesium alloys to structural components in aerospace [4] and ground vehicles [5] is increasing due to the successfully developed new magnesium alloys and its metal-matrix composites that offer excellent properties such as low density, high specific strength and stiffness, good machinability and castability, etc. However, in order to use magnesium alloys as a high strength structural components, especially in automobile, aerospace and other transportation industries, it is very important to make their fatigue characteristics clear. Until now, there has been growing interest in studies on fatigue behavior of magnesium alloys. These include crack growth behavior in die cast AZ91D [6], low cycle fatigue behavior of die cast AZ91E-T6 [7] and fatigue behavior of die cast AZ91 in very high cycle regime (~10^9 cycles) [8]. Hilpert and Wagner examined the fatigue performance of extruded high strength magnesium alloy AZ80 in ambient air as well as an aggressive environment using spray tests with aqueous *NaCl* solution [9]. It was found that there was no significant effect of *NaCl* solution on fatigue life at higher stress amplitudes but fatigue life was considerably reduced at stresses below 125 MPa, which was the fatigue limit in ambient air.

Since magnesium demonstrates poor corrosion resistance and is very sensitive to environment, significant effect on fatigue strength is speculated with changes in frequency and stress ratio. In the previous study, it is clear that the fatigue strength of magnesium alloys significantly decreased at stresses lower than the fatigue limit and highly sensitive to the high humidity levels present in the ambient environment [10]. However, to the authors' best knowledge, there has not been any study reported on the effect of frequency on corrosion fatigue and fatigue crack growth behavior of magnesium alloy. Therefore, it is very important to investigate the effect of frequency especially at high humidity environment.

2.0 EXPERIMENTAL PROCEDURES

The material used was extruded AZ61 (Mg-6%Al-1%Zn) magnesium alloy. The microstructure of the cross-sectional plane of the specimen is shown in Figure 1. Prior to the fatigue tests, tensile properties of extruded AZ61 were evaluated under 20℃-55%RH and 50℃-80%RH. No significant effect of environment on tensile properties was found on magnesium alloy as shown in Table 1.

Fatigue strength tests of extruded AZ61 magnesium alloy were carried out using round bar specimens in an environmental chamber, and the temperature and humidity were controlled to be at 50°C and 80%RH, respectively. Fatigue loading was applied by using sinusoidal waveform with a stress ratio of R=-1 and at the frequencies of 1 and 10Hz. Specimens with threaded end (Figure 2) were machined from the received round bar material (ϕ 15mm) and then polished in the longitudinal direction of the specimen with 500 to 1500 grit emery papers. The gauge length and diameter of the specimen were 6mm and 3mm, respectively.

A centre-cracked tension (CCT) specimen was used for fatigue crack growth test. A screw type fixture was used so that tension-compression loading can be applied. Figure 3 shows the CCT specimen geometry according to ASTM E647-95a standard [11]. To avoid excessive lateral deflection or buckling of CCT specimen during the test, the gauge length and thickness of gauge part were limited to 12 mm and 2 mm, respectively. The gauge part was polished with 500 to 1500 grit emery papers to obtain a smooth surface. An EDM (electrical discharge machining) notch was introduced to facilitate fatigue pre-cracking. The stress ratio R during pre-cracking was the same as the stress ratio used in the fatigue crack growth test. The pre-cracking was stopped after a pre-crack length equal to $0.1B$ (B is the thickness of gauge part) was attained at crack growth rates less than 10^{-8} m/cycle. Fatigue crack growth tests were conducted on a servo-hydraulic testing machine with a maximum capacity of 10kN. The tests were performed under a load control with sinusoidal wave form of stress ratio R= - 1 at a frequency of 1 and 10Hz. The loading direction is in the extrusion direction of the material. The tests were done under the conditions of 20℃-55%RH and 50℃-80%RH.

Crack growth curve (crack growth rate da/dN vs. stress intensity factor range ΔK) was obtained by K-decreasing and K-increasing test procedure. At each load level, the crack was grown more than the plastic zone size corresponding to the previous stress intensity value. The decreasing and increasing load steps are below 10% of the previous loading. The crack lengths were measured on the front and back surfaces of the specimen by a

replica technique.

Table 1: Tensile properties if the extruded AZ61 alloy

	E (GPa)	$\sigma_{0.2\%}$ (MPa)	σ_{UTS} (MPa)	Elongation (%)
20℃-55%RH	43	244	329	23
50℃-80%RH	44	240	326	28

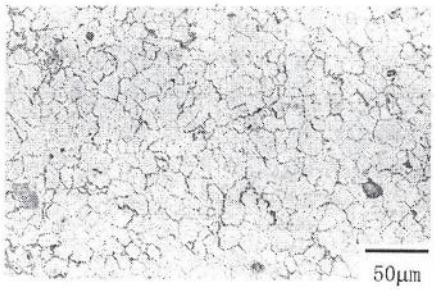

Figure 1: Microstructure of the AZ61 alloy

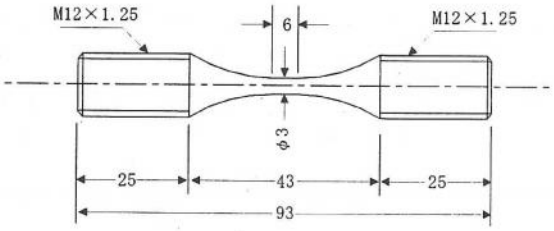

Figure 2: Fatigue test specimen

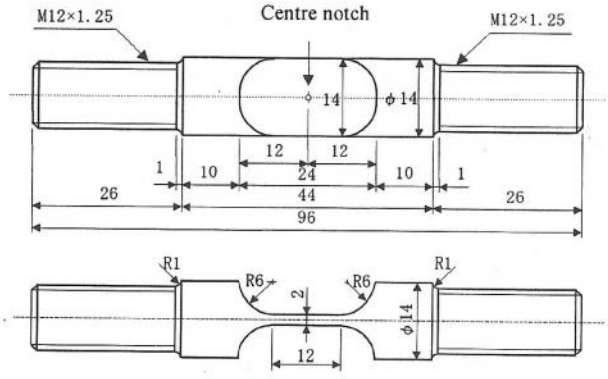

Figure 3: Fatigue crack growth test specimen

The stress intensity factor value for CCT specimen was calculated according to the following equation:

$$K = \sigma\sqrt{\pi a} \cdot F(\alpha) \tag{1}$$

Here, F is a boundary correction factor which depends on the ratio of crack length a to the width of the specimen W. For the CCT test specimen used in this study, the boundary correction factor is given as [12],

$$F = \left(1 - 0.025\alpha^2 + 0.06\alpha^4\right)\sqrt{\sec\left(\frac{\alpha\pi}{2}\right)} \tag{2}$$

where α is

$$\alpha = \frac{2a}{W} \tag{3}$$

The stress intensity factor range ΔK is

$$\Delta K = K_{max} - K_{min} = \Delta\sigma\sqrt{\pi a} \cdot F(\alpha) \tag{4}$$

where

$$K_{max} = \sigma_{max}\sqrt{\pi a} \cdot F(\alpha), \quad K_{min} = \sigma_{min}\sqrt{\pi a} \cdot F(\alpha) \tag{5}$$

The load range ΔP can be expressed as

$$\Delta P = P_{max} - P_{min} \tag{6}$$

Load ratio R is defined as

$$R = \frac{K_{min}}{K_{max}} = \frac{P_{min}}{P_{max}} \tag{7}$$

The crack length increments Δa in each step was according to the ASTM standard, which can be expressed as

$$\Delta a \geq \frac{3}{\pi}\left(\frac{K_{max}'}{\sigma_{ys}}\right)^2 \tag{8}$$

where K_{max}' is the terminal value of K_{max} from the previous load step. The effective stress intensity factor range ΔK_{eff} is defined as

$$\Delta K_{eff} = K_{max} - K_{op} = U \cdot \Delta K \tag{9}$$

Here, K_{max} is the stress intensity factor calculated from the maximum load and K_{op} is the stress intensity value at the minimum load at which the crack is open (opening load, P_o). U is the effective stress intensity range ratio or the crack opening ratio. Crack opening ratio U can be expressed as

$$U = \Delta K_{eff} / \Delta K \tag{10}$$

Equation (9) implies that only the load range between the opening load and the maximum load affects the fatigue crack growth rate.

To determine the crack opening load, two strain gauges were mounted in front of the crack tip on the specimen surface and back surface to detect the crack opening load. Compliance technique (slope of the strain against load curve) has been used to determine the opening load as shown in Figure 4.

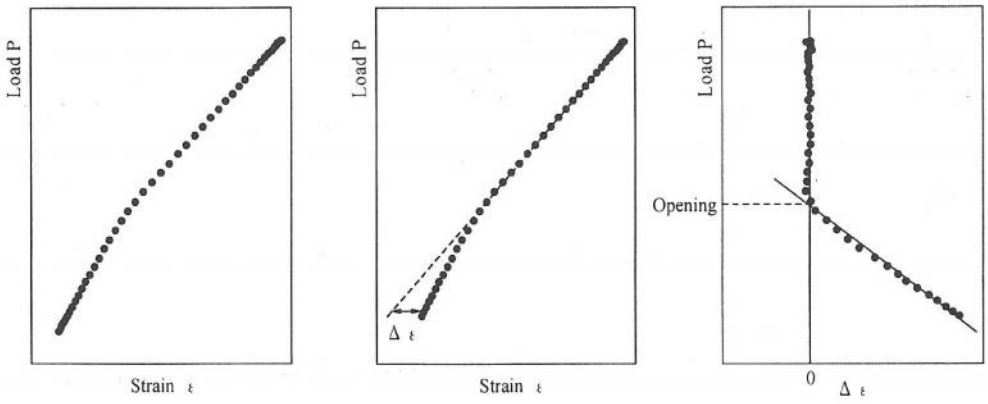

Figure 4: Determination of opening load using the compliance method

3.0 RESULT AND DISCUSSION

3.1 Effect of Frequency on Fatigue Strength

Relationship between stress amplitude and time to failure for the frequencies 1 and 10 Hz is shown in Figure 5. The subscript 'P' adjacent to the data points represents the fatigue crack that nucleated from a corrosion pit. The figure shows that at stresses below the fatigue limit, fatigue life for both frequencies were almost identical.

This suggests that time dependent fatigue fracture was predominant in the stress region lower than the fatigue limit. In contrast, when the same experimental data points were re-plotted as a function of number of cycles to failure as shown in Figure 6, the S-N curves for stresses higher than the fatigue limit were in one narrow band regardless of frequencies. Therefore, it is suggested that the fatigue fracture in the region higher than the fatigue limit was predominantly cyclic dependent.

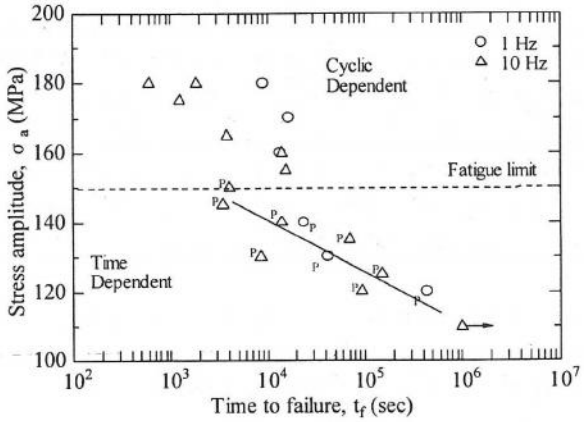

Figure 5: Relationship between stress amplitude and time to failure

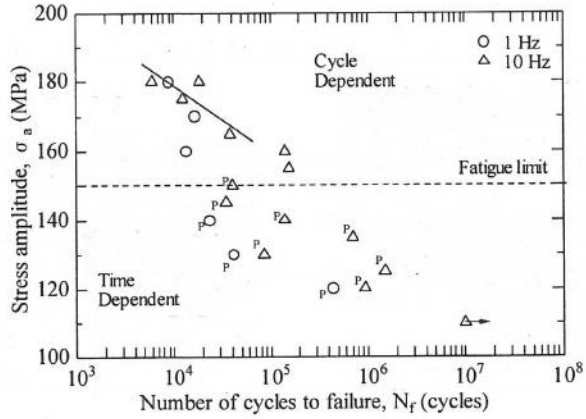

Figure 6: Relationship between stress amplitude and number of cycles to failure

3.2 Fracture Surface Observations

Figure 7 shows scanning electron microscope (SEM) observations of fracture surface for the specimen tested at 130MPa under the frequency of 1 and 10 Hz. Both the fatigue fracture origin of AZ61 tested at low stresses at 50℃ -80%RH environment can clearly identify to be nucleated from a corrosion pit. For all the specimens failed at stress amplitudes lower than the fatigue limit, a similar fracture surface morphology was observed in both 1 and 10 Hz specimens, which showed the existence of corrosion pit at the fracture origin. The corrosion pit size observed for the 1 Hz specimens was about $30-70\ \mu$ m. This size was larger compared to the pit size observed for the 10 Hz

specimens that was about $20-30\ \mu$ m.

In contrast, no evidence of corrosion pit was found at the fatigue crack nucleation site for the specimens failed at stress amplitudes higher than the fatigue limit, as shown in Figure 8. The fracture origin was relatively flat for both specimens tested at the frequencies of 1 and 10 Hz. This implies that at stresses higher than the fatigue limit, the cyclic dependent slip deformation (intrusion and extrusion) was more severe compared to the time dependent corrosion process, consequently leads to fatigue crack nucleation in 1 and 10 Hz specimens.

SEM observation was also carried out on the specimen surface to search for the evidence of corrosion pit. Figure 9 (a) shows the early stage of corrosion pit formation where corrosion products were observed on the surface of specimen tested at 130 MPa. From the figure, it can be seen that many cracks appeared around the corrosion product. Yamamoto et al. suggested that when corrosion product formed on magnesium surface, shrinkage occurs, which leads to the crack nucleation in the corrosion product [13]. This corrosion product may detach from the specimen surface

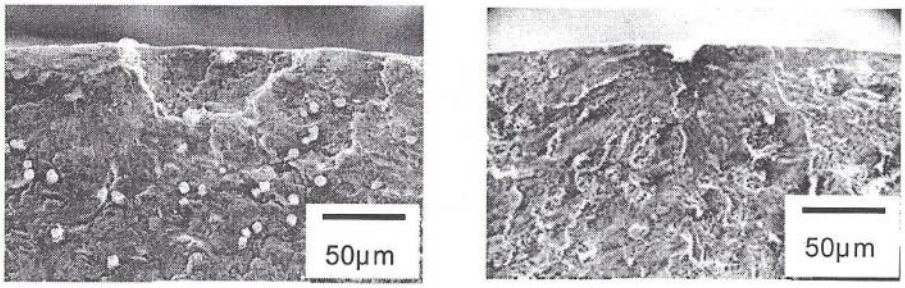

(a) 1 Hz (b) 10 Hz

Figure 7: SEM fractographs showing a corrosion pit in specimen tested at 130 MPa under 1 and 10 Hz at 50°C-80 %RH

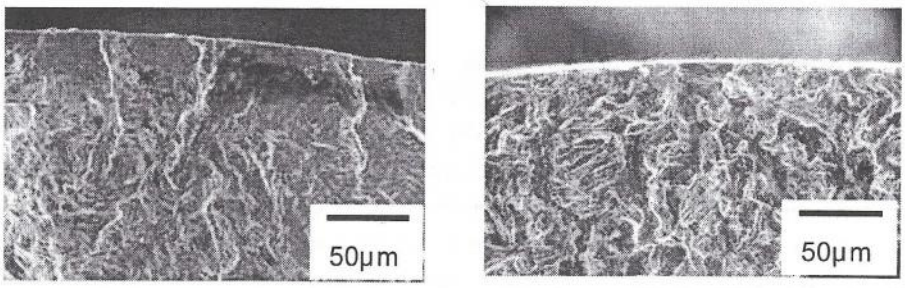

(a) 1 Hz (b) 10 Hz

Figure 8: SEM fractographs showing the fatigue crack initiation site of specimen tested at 180 MPa under 1 and 10 Hz at 50°C-80 %RH. No evidence of corrosion pit was observed

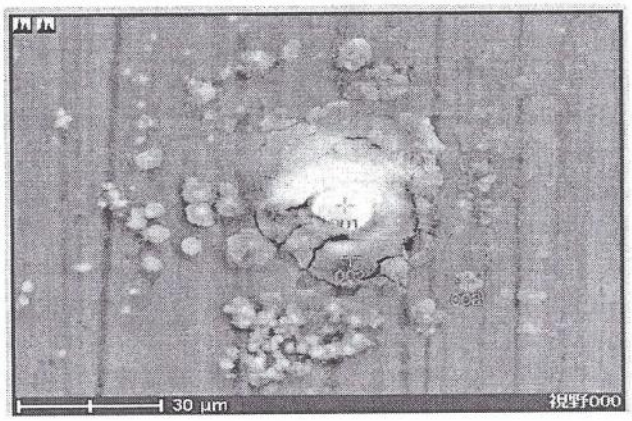

(a) SEM image

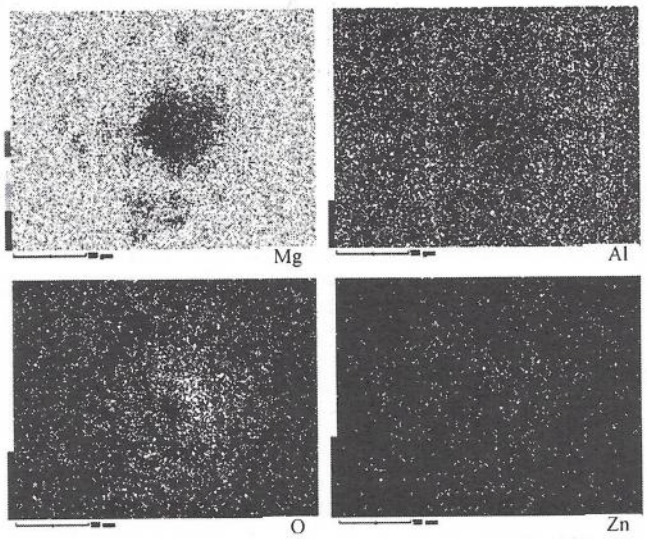

(b) EDS mapping analysis

Figure 9: SEM observation and EDS mapping analysis of corrosion product on the specimen surface

and form a pit. The corrosion product was analyzed by using an energy dispersive spectroscopy (EDS) to identify its elements. Figure 9 (b) shows the result of EDS mapping analysis of the corrosion product, respectively. It was found that the corrosion product mainly consisted of magnesium and oxygen.

3.3 Corrosion Pit Formation Mechanism

Initiation of pitting corrosion under cyclic loading condition may be caused by material/environment/cyclic loading combination [14]. Thin oxide layers (MgO) naturally formed on the specimen surface of magnesium alloy, when the surface exposed to ambient air. This protective film provides a corrosion protection to underlying material.

The mechanism of corrosion pit formation in magnesium alloy at high humidity environment is illustrated in Figure 10. Under cyclic loading, cumulative plastic strains that lead to formation of rough surface due to extrusion and intrusion of persistent slip bands break down the thin protective film on magnesium alloys surface. Electrochemical attack occurs at the localized breakdown site, where the less-deformed surrounding area will behave as cathode. In contrast, deformed area will behave as anode and forms a pit. If the opening or crevice caused by the breakdown of the thin oxide layer is wide enough to permit the condensed water-droplets to enter into the underlying metal, crevice corrosion may occur [15]. If the water-droplets enter the opening, magnesium hydroxide formed and the electrochemical reactions involved during the pitting are as follows:

$$Mg + 2(OH)^- \rightarrow Mg(OH)_2 + 2e^- \quad \text{(Oxidation)} \qquad (11)$$

$$2H_2O + 2e^- \rightarrow 2(OH)^- + H_2 \quad \text{(Reduction)} \qquad (12)$$

If no water droplets enter the opening, the magnesium metal may react with the oxygen to form magnesium oxide. The electrochemical reactions involved are:

$$2Mg + O^{2-} \rightarrow 2MgO + 4e^- \quad \text{(Oxidation)} \qquad (13)$$

$$O_2 + 4e^- \rightarrow 2O^{2-} \quad \text{(Reduction)} \qquad (14)$$

Once a pit forms, stress concentration occurs at the root of the pit and enhances pit growth to the critical pit size. Consequently, it is suggested that, the conjoint action between localized plastic deformation due to cyclic load and environment leads to formation of pit and subsequent fatigue crack initiation under high humidity condition at stresses below the fatigue limit. On the other hand, at stresses higher than the fatigue limit, the localized plastic deformation is much more significant and directly leads to fatigue crack initiation, where the crack initiation is faster compared to the corrosion pit formation.

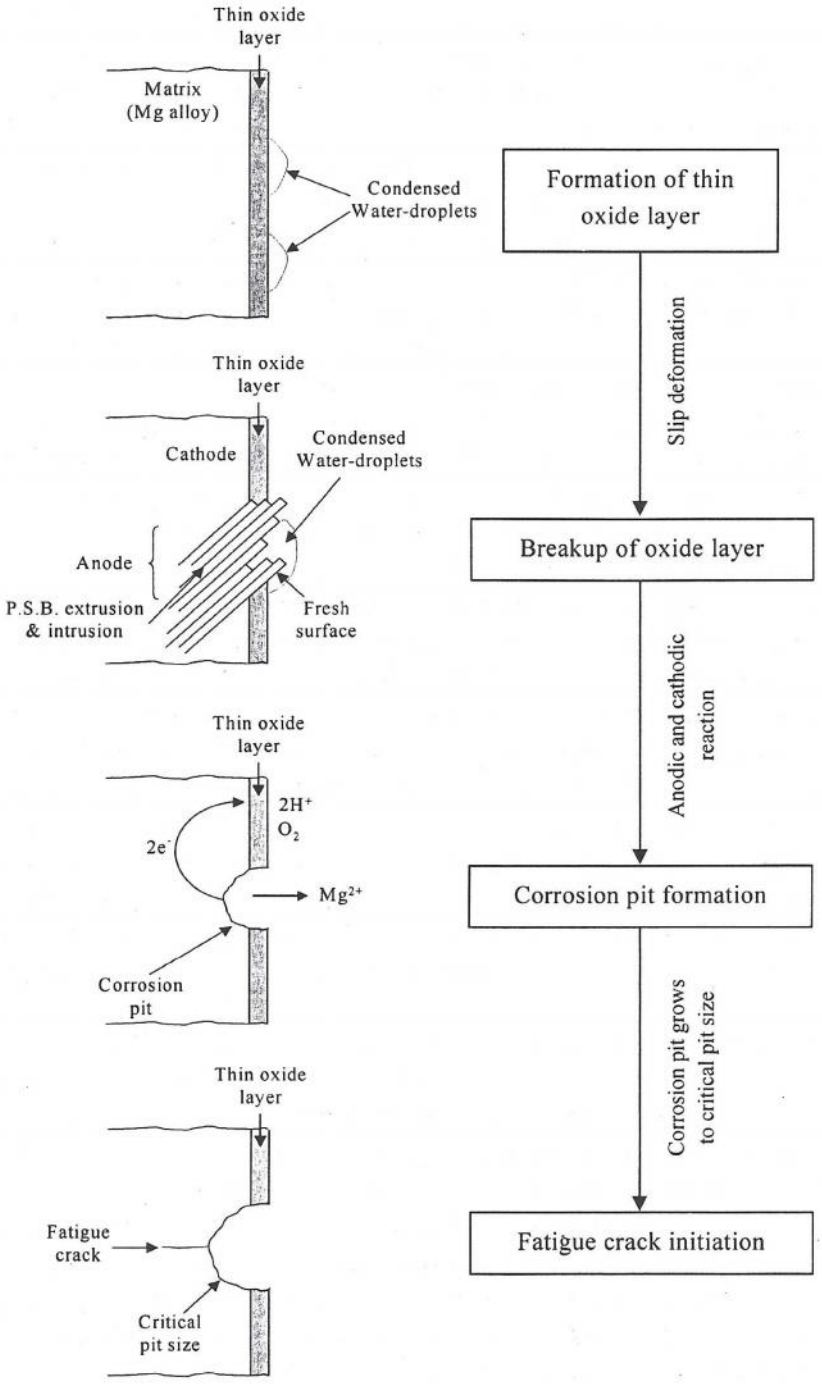

Figure 10: The illustration of corrosion pit formation mechanism and fatigue crack initiation in magnesium alloy at high humidity environment

3.4 Effect of Frequency on Fatigue Crack Growth Behavior

Figure 11 shows the effect of frequency on fatigue crack growth behavior of AZ61 magnesium alloy at 50℃-80%RH. The tests were carried out according to the K-decreasing and K-increasing testing method. Vertical axis is the fatigue crack growth rate and horizontal axis is the stress intensity factor range. Arrows in the figure indicate the threshold value of stress intensity factor range ΔK_{th}. In the figure, circle and triangle symbols represent the 1 and 10 Hz data, respectively. Open and close marks represent stress intensity factor range ΔK and effective stress intensity factor range ΔK_{eff}, respectively. From the results, it was found that at high stress intensity region, the fatigue crack growth curve for 1 Hz showed a slightly higher crack growth rate compared to that for 10 Hz. However, the difference becomes smaller with decreasing ΔK, and the fatigue crack growth rates for 1 and 10 Hz were reversed at stress intensity factor lower than 4 MPa.m$^{1/2}$. At the near-threshold region, 1 Hz demonstrated higher fatigue crack growth resistance compare to the 10 Hz specimens. The threshold value of stress intensity factor range ΔK_{th} for 1 and 10 Hz were 2.37 and 1.3 MPa.m$^{1/2}$, respectively.

From the fatigue test results, it is speculated that the observed corrosion pit size in 1 Hz specimen, which was larger than that in the 10 Hz specimen, may be due to the higher threshold stress intensity factor and fatigue crack growth resistance in the 1 Hz specimen. It is assumed that a fatigue crack nucleates from a corrosion pit when the pit grows to a critical size at which the stress intensity factor reaches the threshold value [9]. Since the threshold value was higher, larger corrosion pit size was required for fatigue crack nucleation in the 1 Hz specimen. Therefore, it is suggested that the fatigue life for 1 Hz specimen was mainly dominated by the corrosion pit formation and the early crack growth after the crack nucleation. The crack propagation is speculated to be short since the fatigue crack growth rate was high at higher stress intensity factor range.

The relationship between crack opening ratio U and stress intensity factor range ΔK for 1 and 10 Hz is shown in Figure 12. From the figure, it is found that the crack opening ratio increased with increasing ΔK in both frequencies. The crack opening ratio for AZ61 becomes constant at 0.5, which indicated that there was no crack closure identified at the tension stress levels. Crack closure behavior was more pronounced in 1 Hz compared to 10 Hz, where the crack closure effect was first identified at ΔK = 4.5 MPa.m$^{1/2}$ for the 1 Hz. The crack closure effect for 10 Hz was first identified at lower ΔK level around 3.0 MPa.m$^{1/2}$. The effect of specimen orientation on the crack opening ratio can be seen at ΔK less than 2 MPa.m$^{1/2}$.

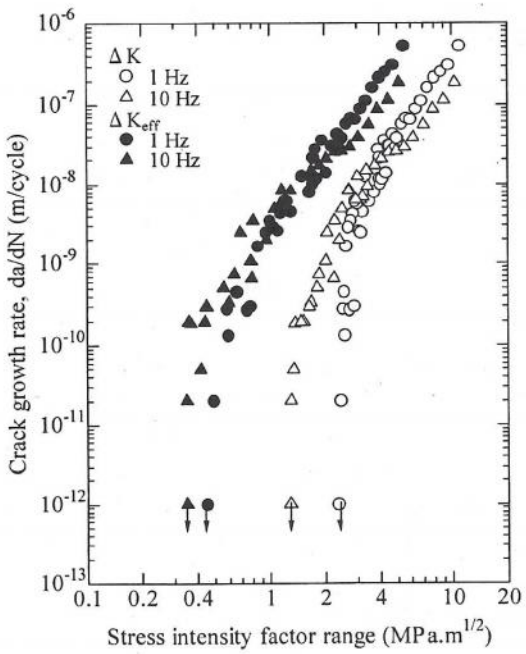

Figure 11: Effect of frequency on fatigue crack growth behavior of AZ61 under 50°C-80%RH

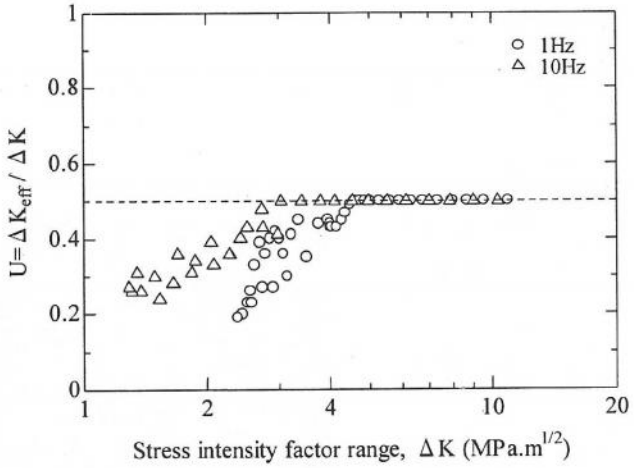

Figure 12: Relationship between crack opening ratio U and stress intensity factor range ΔK

Considering the effect of crack closure, the fatigue crack growth rate as a function of effective stress intensity factor range ΔK_{eff} was super imposed in filled symbols as shown in Figure 11. The figure shows that, at stress intensity

region less than 2 MPa.m$^{1/2}$, regardless of frequency, the fatigue crack growth curves for 1 and 10 Hz coincided in a narrow band. This was due to the more pronounced effect of crack closure in the 1 Hz compared to the 10 Hz. The threshold value of effective stress intensity factor range $\Delta K_{eff,th}$ was around 0.4 MPa.m$^{1/2}$. This indicates that the ΔK_{eff} is the intrinsic driving force for fatigue crack growth in both 1 and 10 Hz frequencies. At ΔK higher than 2 MPa.m$^{1/2}$, the *da/dN*- ΔK_{eff} curve for 1 Hz showed higher crack growth rate than 10 Hz, same as in the *da/dN*- ΔK curve.

The pronounced crack closure effect in 1 Hz compared to that in 10 Hz was due to the oxide-induced crack closure. In 1 Hz crack growth test, the exposed time of crack surface to the high humidity environment, i.e. the time for the formation oxide layer was 10 times longer compared to that in 10 Hz. The presence of oxide layer on the crack surface was identified from the EDS surface analysis as shown in Table 2. The result indicated that oxygen was detected on the entire crack surface especially in the crack wake at the near-threshold region. The quantitative analysis showed that about 98% of the intermetallic compound was MgO.

Table 2: The EDS surface and quantitative analysis

Element	(keV)	Mass %	Error %	Atomic %	Intermetallic	Mass %
O	0.000	39.82	0.00	0.00		0.00
Mg K	1.253	59.23	1.41	99.28	MgO	98.20
Al K	1.486	0.95	3.61	0.72	Al203	1.80
		100.00		100.00		100.00

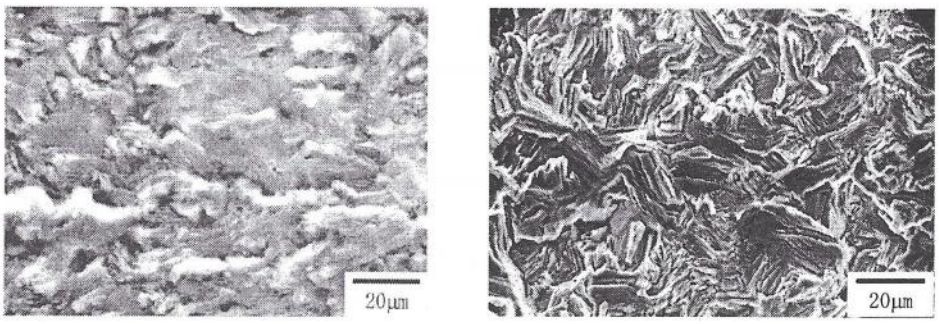

(a) 1 Hz (b) 10 Hz

Figure 13: Crack surface of specimen tested under 1 and 10 Hz frequency

The SEM observation result of crack surface for 10 Hz is shown in Figure 13. The figure shows that the oxide layer that covered the crack surface was less compared to that in the crack surface of the 1 Hz. It is assumed that the oxide layer on the crack surface in the 1 Hz was thicker than in the 10 Hz, i.e. more pronounced crack closure effect observed in the 1 Hz as shown in Figure 12. In the high stress intensity factor region, where the crack closure was not identified at the tension stress levels, the fatigue crack growth rate in the 1 Hz was higher than in the 10 Hz in both da/dN- ΔK and da/dN- ΔK_{eff} curves. This phenomenon could be related to the difference in the thickness of oxide layer (MgO) formed in front of the crack. The MgO oxide layer is brittle and easy to break. Ishikawa et al. suggested that the thicker the oxide layer the longer the crack propagates in one cycle loading [16]. The oxide layer formed under low frequency was thicker than that in high frequency so that the effective crack length is longer under lower frequency and results in higher fatigue crack growth rate.

4.0 CONCLUSION

Effect of frequency on fatigue and fatigue crack growth behavior for AZ61 magnesium alloy was investigated in high humidity environmental condition. Summaries of this chapter are as follows:

1) The fatigue property of AZ61 magnesium alloy in high humidity was affected by loading frequency. At stress amplitudes below the fatigue limit, fatigue fracture was predominantly time dependent behavior where the S-N curves for 1 and 10 Hz were in one narrow band. In opposite, at stresses higher than the fatigue limit, fatigue fracture was predominantly cyclic dependent behavior.
2) Fatigue fracture at low stress amplitudes under both 1 and 10 Hz were originated from the corrosion pit formed at the surface. However, the pit size in 1 Hz specimen was larger because the threshold value was higher, i.e. larger corrosion pit size was required for fatigue crack nucleation compared to that in the 10 Hz specimen. The fatigue life for 1 Hz specimen will be mainly dominated by the corrosion pit formation and the early crack growth after the crack nucleation.
3) Specimen tested at frequency of 1 Hz demonstrated higher fatigue crack growth resistance compare to that of 10 Hz at the near-threshold region due to the pronounced oxide-induced crack closure effect in 1 Hz compared to that in 10 Hz.

REFERENCES

1. Schubert, E., Klassen, M., Zerner, I., Walz, C. and Sepold, G., 2001, Light-Weight Structures Produced by Laser Beam Joint For Future Application in Automobile and Aerospace Industry, *J. Mat. Processing Tech.*, 115: 2-8.
2. Mordike, B.L. and Ebert, T., 2001, Magnesium: Properties-applications-potential, *Mat. Science Engineering,* A302: 37-45.
3. King, J.F., Fowler, G.A. and Lyon, P., 1991, Corrosion Resistant Magnesium Alloy for Aerospace Casting, *Light Weight Alloys for Aerospace Applications II, The Minerals, Metals & Materials Society*, 423-438.
4. Duffy, L., 1996, Magnesium alloys: the light choice for aerospace, *Material World*: 127-130.
5. Luo, A.A., 2003, Recent Magnesium Alloy Development for Automotive Powertrain Applications, *Mat. Science Forum,* 419-422: 57-66.
6. Shibusawa, T., Kobayashi, Y. and Ishikawa, K., 1997, Fatigue Crack Propagation in Die Cast AZ91D Magnesium Alloy, *J. Japan Inst. Metal*, 61(4): 298-302.
7. Goodenberger, D.L. and Stephens, J.R.I., 1993, Fatigue of AZ91E-T6 Cast Magnesium Alloy, *Engineering Mat. Technology,* 115: 391-397.
8. Mayer, H.R., Lipowsky, Hj., Papakyriacau, M., Rosch, R., Stich, A. and Stanzl-Tschegg, S., 1999, Application of Ultrasound for Fatigue Testing of Lightweight Alloys, *Fatigue Fract Engineering Mat. Struct,* 22: 591-599.
9. Hilpert, M. and Wagner, L., 2000, Corrosion Fatigue Behavior of the High-Strength Magnesium Alloy AZ80, *J. Mat. Engineering and Performance,* 9 (4): 402-407.
10. Sajuri, Z.B., Miyashita, Y. and Mutoh, Y., 2005, Effects of Humidity and Temperature on Fatigue Behavior of an Extruded AZ61 Magnesium Alloy, *Fatigue Fract Engineering Mat. Struct*, 28: 373-379.
11. ASTM Standard ASTM E647-95a, 1998, Annual Book of ASTM Standard, 3 (1): pp.562.
12. Murakami, Y. (Editor-in-chief), 1987, Stress Intensity Factors Handbook, Vol.1, Pergamon Press: pp. 3.
13. Yamamoto, A. and Tsubakino, H., 2003, A New Technique For Surface Modification in Magnesium Alloy by Applying Magnesium Oxide Coating, *Mat. Sc. Forum,* 419-422: 903-908.
14. Hoeppner, D.W., 1979, Model For Prediction of Fatigue Life Based on a Fitting Corrosion Fatigue Process, *Fatigue Mechanisms*, ASTM STP 675, ASTM, Philadelphia: 841-870.

15. Vera, R., Rosales, B.M. and Tapia, C., 2003, Effect of the exposure angle in the corrosion rate of plain carbon steel in a marine atmosphere, *Corrosion Science*, 45: 321-337.
16. Ishikawa, K., Kobayashi, Y. and Ito, T., 1995, Characteristics of Fatigue Crack Propagation in Heat Treatable Die Cast Magnesium Alloy, *Light Weight Alloys for Aerospace Applications III, The Minerals, Metals & Materials Society*, 449-462.